Performance of Welded High-Strength Low-Alloy Steels in Sour Environments

G.M. Omweg, G.S. Frankel,‡,* W.A. Bruce,** J.E. Ramirez,** and G. Koch****

ABSTRACT

Sulfide stress cracking (SSC) susceptibility of gas metal arc welded API 5L X70 and X80 line pipe steel was tested using standard and modified NACE TM0177 (Method A) testing. Two applied stresses and three concentrations of dissolved hydrogen sulfide (H_2S) were used. The effect of peak weld hardness was examined by using three weld conditions. Several welds meeting the HRC 22 requirement failed by SSC. Welds containing hardness exceeding 248 HV were resistant to SSC at low H_2S concentrations. The centerline segregation region (CSR) observed in the X70 pipe steel played an important role in the SSC and hydrogen-induced cracking (HIC) susceptibility of the welds. The X80 material was more susceptible at lower hardness values due to localized softening during welding, and subsequent plastic deformation upon loading. An extrapolation to in-service weldments indicated that the NACE MR0175 requirements may be conservative for high-strength low-alloy steel welds not in direct contact with the sour environment.

KEY WORDS: hydrogen embrittlement, hydrogen sulfide cracking test, pipelines, steel, sulfide stress cracking, weld

INTRODUCTION

Steels with hardness higher than HRC 22 have been shown to be susceptible to sulfide stress cracking (SSC), a form of hydrogen embrittlement (HE),[1-3] in sour service environments. The suitable sour service materials listed in NACE MR0175[4] are based on their resistance to SSC either in actual field applications or on laboratory testing performed using the NACE TM0177 test method, which is a severe, accelerated exposure test.[5] Many high-strength low-alloy (HSLA) steels are precluded from NACE MR0175, especially in the as-welded condition, due to either high parent material hardness or to the formation of localized high-hardness weld regions in the weld heat-affected zone (HAZ). HAZ regions have exhibited high susceptibility to SSC in both service and laboratory environments.[2] Because of the inherent toughness afforded by HSLA steels, the NACE MR0175 requirement may be overly conservative for this class of alloys.

Oil and gas transport conditions are becoming increasingly sour (higher hydrogen sulfide [H_2S] concentrations) and the use of higher strength HSLA grades is prevented where NACE MR0175 is used as a governmental regulation. The performance of pipeline girth welds used to connect pipe segments in the field is of interest. Multi-pass circumferential girth welds cause tempering in underlying hard HAZ regions, leaving the hardest HAZ regions in the final untempered cap passes. On the pipeline exterior, welds are exposed to lower hydrogen concentrations

Submitted for publication April 2002; in revised form, January 2003. Presented as paper no. 02048 at CORROSION 2002, April 2002, Denver, CO.

‡ Corresponding author.
* Fontana Corrosion Center, The Ohio State University, 477 Watts Hall, 2041 College Rd., Columbus, OH 43210.
** Edison Welding Institute, 1250 Arthur E. Adams Dr., Columbus, OH 43221.
*** CC Technologies, Inc., 6141 Avery Rd., Dublin, OH 43016.

0010-9312/03/000127/$5.00+$0.50/0

TABLE 1
Base Alloy Compositions and Pipe Dimensions

API 5L Steel Pipeline Compositions (wt%) and Dimensions																	
Alloy	**C**	**Mn**	**P**	**S**	**Si**	**Ni**	**Cr**	**Mo**	**Cu**	**V**	**Al**	**Ti**	**Nb**	**CE_{IIW}**	**Pcm**	**OD[(A)]**	**t[(A)]**
X70	0.16	1.6	0.013	<0.003	0.32	<0.01	0.02	<0.01	0.01	0.08	0.03	0.01	0.04	0.47	0.26	34.75	0.75
X80	0.029	1.86	0.008	0.003	0.35	0.11	0.06	0.25	0.22	<0.005	0.03	0.02	0.10	0.45	0.170	42	0.55

[(A)] Measurements in inches.

than weld regions in contact with the sour environment on the inner pipe surface. SSC is a HE mechanism, so higher hardness values (exceeding HRC 22) should be tolerable in hard weld cap regions, which are exposed to relatively low hydrogen concentrations. In fact, it has been shown that hard external weld regions exceeding 300 HV (248 HV = HRC 22) were resistant to SSC in a stressed pipe filled with the NACE test solution.[6] This investigation was aimed at assessing the conservatism of the NACE requirements for HSLA weldments. Aspects of this work focused on welding parameters and microstructure are given elsewhere.[7-8]

EXPERIMENTAL PROCEDURES

The materials investigated were API 5L X70 and X80 spiral-welded HSLA line pipe materials. These alloys are designated by their specified minimum yield strength (e.g., YS for X70 is 70 ksi). The compositions of the alloys are given in Table 1 along with values of carbon equivalents CE_{IIW} and Pcm, and the pertinent pipe dimensions, including outer diameter (OD) and wall thickness (t). The carbon equivalent is convenient for comparing the weldability of different steels. The X80 was very low in carbon, just above saturation in ferrite (0.022 wt% C) at the eutectoid temperature. Both alloys were low-sulfur steels.[9] The primary carbo-nitride (CN) forming elements in the X70 and X80 were vanadium and niobium, respectively.

The as-received microstructure of the X70 pipe steel consisted of banded, fine-grained ferrite + pearlite as shown by the long transverse section in Figure 1(a). The X70 pipe steel contained a heavily banded centerline segregation region (CSR) characterized by thicker, more continuous banding, as shown in Figure 1(b). The CSR region was compositionally different due to segregation of elements like C and Mn.[10] As a result, the alloy-rich bands are more hardenable than the alloy-lean bands. In contrast, the X80 did not contain large amounts of carbide, a banded microstructure, or a visible CSR. Figure 2 reveals fine-grained ferrite, large secondary ferrite grains, and granular bainite in the X80 parent material. Although susceptibility to SSC generally increases with increasing hardness, some microstructures are more susceptible to cracking than others at the same hardness. For example, tempered martensite is more resistant than tempered bainite or mixed microstructure at the same hardness level. The observed differences in microstructure between X70 and X80 steel pipes is a result of different chemical compositions and different steel processing routes.

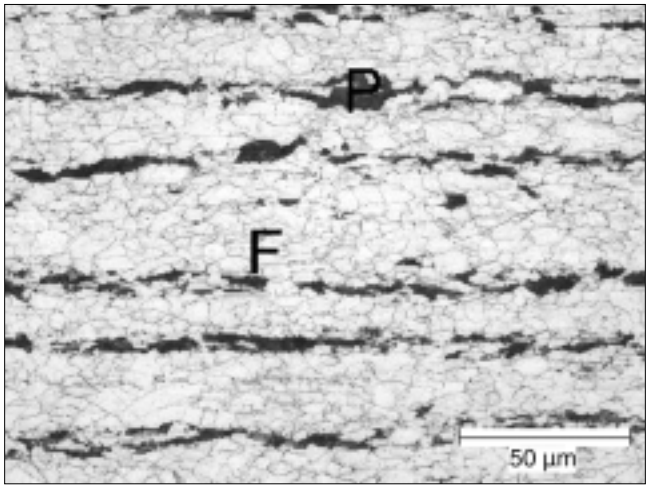

(a)

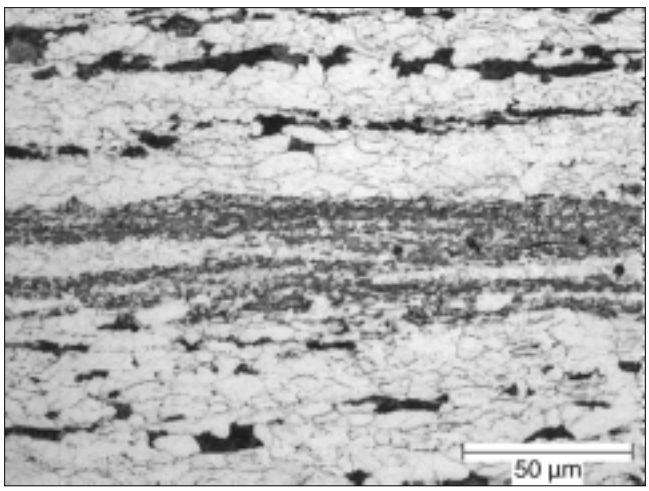

(b)

FIGURE 1. *X70 long transverse section, 2% nital etch (a) fine grained ferrite (F) and pearlite bands (P) and (b) CSR.*

The through-wall hardness profile of each pipeline steel was measured using the Rockwell C and Vickers 10-kg hardness test methods. Neither parent material exceeded HRC 22.[8]

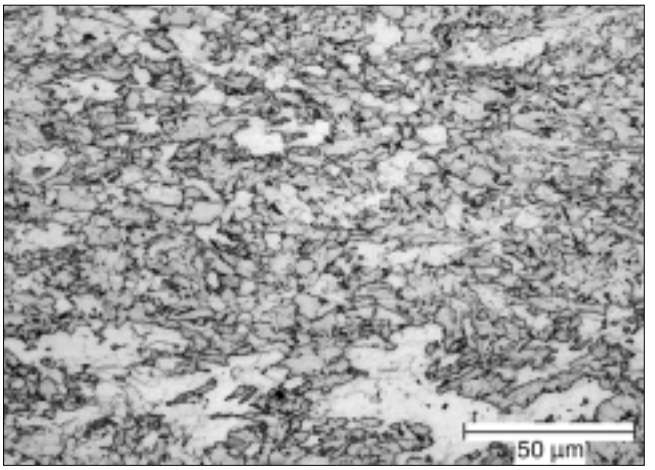

FIGURE 2. *X80 long transverse section, 2% nital etch.*

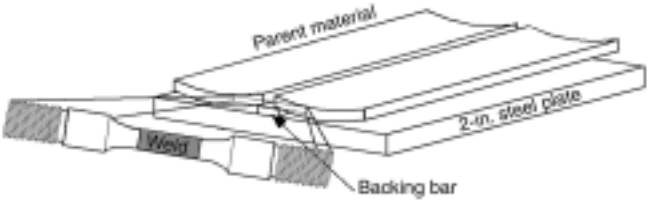

FIGURE 3. *Schematic of setup for welding of plates to simulate girth welds.*

Because of difficulties in making actual girth welds on large pipe sections without the proper automated gas metal arc welding (GMAW) equipment, simulated girth welds were used for this work. Two 6-in.-by-24-in. (15.2-cm-by-61-cm) unflattened plates cut from the pipe stock were utilized for each joint. The plates were tack-welded to a 2-in. (5.1-cm)-thick steel plate to provide the necessary constraint during cooling. A schematic of the weld geometry is shown in Figure 3. The joint geometry was chosen to duplicate a typical girth weld joint: a 0.25-in. (0.64-cm) root gap with a 12° included angle. All root passes were deposited using low arc energy (15.1 kJ/in. [5.9 kJ/cm]). The subsequent fill passes created the gauge material isolated in the tensile specimens for SSC testing. The fill pass weld preheat and input energy were varied to achieve three desired ranges in specimen peak hardness for each steel pipe. These parameters were chosen based on the results of preliminary weld trials. Altering the weld preheat and welding parameters changed the weld cooling rate, which, in turn, influenced microstructural evolution in each weld HAZ and fusion zone. The parameters used for the fill passes in each weld condition appear in Table 2. Condition I, II, and III welds correspond to hard, medium, and soft gauge regions, respectively, in the final simulated girth welds.

Low-heat input and room temperature (RT) preheat were used for the weld cap passes to minimize tempering effects, thus improving the predictability of the peak hardness from preliminary bead-on-plate weld data. Cap passes were omitted from all Condition III welds to prevent localized hard spots in these softest weld conditions.

The welds were performed using an automated GMAW station, which allowed for accurate control of the weld travel speed. The pertinent welding process parameters common to all welds (both X70 and X80) appear in Table 3. The typical composition for the ER 70S-3 filler metal wire is 0.08% C, 1.1% Mn, and 0.6% Si. The joints were milled flat on the upper and lower surfaces and cut into plates for radiographic defect screening. Transverse weld tensile test specimens were machined in accordance with the specifications in NACE TM0177-A. The weld metal region was centered in the gauge length of the tensile specimens as shown schematically in Figure 3. Hardness mapping across each weld was performed to system-

TABLE 2
Welding Parameters and Hardness Mapping Results

Weld Condition	Relative Peak Hardness	Voltage (V)	Current (A)	Travel Speed (in./min)	Energy Input (kJ/in.)	Preheat (°F)	Hardness Range (HV 10 kg)	Peak Hardness (HV 10 kg)	Peak Hardness HRC	Peak HV Converted to HRC
X70 Condition I	High	23	172	15.7	15.1	RT[A]	189 to 295	295	<20	29.1
X70 Condition II	Medium	23	172	15.7	15.1	250	185 to 269	269	<20	25.3
X70 Condition III	Low	33	300	14.6	40.7	250	154 to 236	236	<20	19.8
X80 Condition I	High	23	172	15.7	15.1	RT	190 to 293	293	20.2	28.8
X80 Condition II	Medium	23	172	15.7	15.1	250	199 to 286	286	<20	27.8
X80 Condition III	Low	33	300	14.6	40.7	250	179 to 247	247	<20	21.8

[A] Room temperature.

atically quantify both the peak weld hardness and hardness distribution in the tensile samples. Specifics concerning the hardness mapping procedure are discussed elsewhere.[7-8]

SSC resistance was evaluated using a test matrix in which weld hardness, applied stress, and H_2S concentration and base material were varied. X70 and X80 plates were welded with three weld conditions to produce a range in specimen peak weld hardness. Two stresses, 80% or 100% of the specified minimum parent yield, were applied to the samples. These high stresses were used to duplicate the high residual tensile stresses encountered in as-welded in-service weldments.[11] The NACE TM0177-A solution was used as a base solution: 5 wt% sodium chloride (NaCl) + 0.5 wt% glacial acetic acid (CH_3COOH) in deionized water.[5] A range in H_2S concentration was achieved by saturating the solution with different gas mixtures: 100%, 30%, or 10% H_2S (balance N_2). The condition of 100% H_2S exactly reproduced the standard NACE TM0177-A test condition, but the H_2S-N_2 mixtures created a major modification. Proving rings were used for static load application and nitrogen was used for solution deaeration. The time-to-failure (TTF) for complete fractures was measured automatically. All testing procedures outlined in NACE TM0177 were followed, except the fact that diluted H_2S gas mixtures were used for several testing schedules. The H_2S testing was performed in a special H_2S lab.

After 720 h (30 days) or complete fracture, each specimen was removed from the respective corrosion cell. Any corrosion product was removed from the shanks of each tensile bar with an abrasive pad. The gauge was not abrasively treated, but was rubbed vigorously by hand with a rubber glove. The mass was measured for weight-loss determination. Dimensional measurements were made on each sample to determine the exposure area for calculation of corrosion rate.[7]

Following specimen removal, each specimen was examined at 10X to find any apparent surface cracking, as specified the NACE TM0177-A standard. Cracking observed at 10X was sectioned and metallographically prepared to determine if SSC was the cause. In addition to the NACE failure criterion, a more detailed cracking investigation was performed (referred to hereafter as "internal investigation"). During the internal investigation, the entire surface of every sample was examined in the scanning electron microscope (SEM), whether or not cracking was observed at 10X. After SEM examination, a flat was then ground on each cylindrical gauge sample, and the depth of each detected crack-like defect was determined relative to the flat using the depth gauge on a dial caliper (Figure 4[a]). Each sample was coated with Ni using an electroless Ni plating bath for edge retention during metallographic examination. Each sample was then mounted such that the ground flat was exposed on the mount surface and then lapped using an automatic polisher until the defect was reached (Figure 4[b]). Specimens without external indications of cracking were systematically sectioned to reveal any possible internal cracking. When possible, the microstructure around internal cracks was hardness tested using the Vickers 10-kg method. In completely fractured samples, SEM examination focused on the fracture surface, in particular, the crack initiation zone, the crack propagation surface, and the final rupture region. The initiation zone was cross-sectioned metallographically. After documentation, each fracture sample was hardness-tested around the brittle initiation and propagation microstructures. Hardness testing in the ductile rupture region was not relevant as severe plastic deformation was evident in this region and hardness values would not reflect the local hardness prior to SSC testing.

Cathodic charging experiments were performed on samples in conditions that resulted in complete failure in the H_2S testing study. Cathodic charging provided a significant source of atomic hydrogen while avoiding the use of H_2S. The hope was to find charging conditions that correlated to the aggressiveness of the H_2S environment by comparing the failure conditions. Testing would be greatly simplified if the use of H_2S were not necessary. The NACE solution without H_2S but containing 2 mg/L of sodium arsenite ($NaASO_2$) was used. The arsenic was added as a cathodic poison. This exact solution was utilized by

TABLE 3
Welding Conditions

Process	Welding Wire	Shielding Gas	Contact-Tip-to-Work-Distance
Automated GMAW	ER70S-3: S-solid wire, 3-med silicon, 0.045 in.	75Ar-25CO_2	3/4 in.

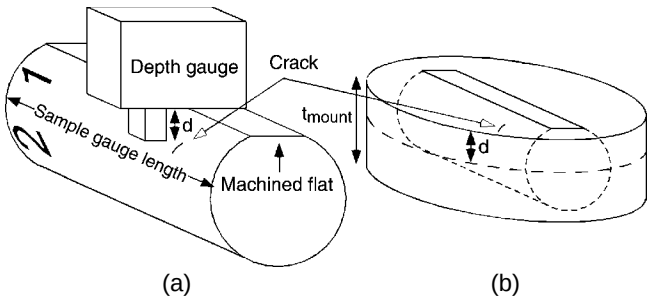

FIGURE 4. *Schematic representation of internal investigation. (a) Determination of depth of cracks relative to flat and (b) mounting and lapping of sample to depth of crack.*

TABLE 4
Cathodic Charging Testing Parameters

Sample	Solution	Applied Stress (%YS)	Δi (μA/cm²)	i_{max} (μA/cm²)
X70 I	NACE + As	100	50	700
X70 II	NACE + As	100	50	700
X70 III	NACE + As	100	25	625
X80 III	NACE + As	100	25	625
X70 I	NACE + As	100	25	850
X80 III	NACE + As	100	25	850
X70 I	NACE	100	50	625
X80 II	NACE	100	50	625
X70 I	NACE + As	100	—	2,000/24 h
X80 II	NACE + As	100	—	2,000/24 h
X70 I	NACE + As	100	—	3,000/24 h
X80 II	NACE + As	100	—	3,000/24 h

Berkowitz and Heubaum to determine the role of hydrogen in SSC.[1] The tensile samples that were used for the cathodic charging evaluation were identical to the SSC specimens. The tensile shanks and fillet regions were masked and the area of the exposed gauge was then determined to specify the applied current density (A/cm^2) in the charging experiments. Samples were loaded into the same type of corrosion cell that was used for the SSC testing. In this case, however, a platinum counter electrode (CE), a Luggin probe/reference electrode (REF) setup, and a dual inlet/outlet bubbler for nitrogen sparging were included. The tensile sample served as the working electrode (WE). The tensile load was applied with a proving ring. The solution was deaerated prior to testing with high-purity N_2 and a constant flow of N_2 was supplied during testing. The applied current density was stepped from an initial value in increments (Δi) of 25 $\mu A/cm^2$ or 50 $\mu A/cm^2$ every 12 h in an attempt to determine the charging current required to cause double-ended fracture for each respective weld condition. It was assumed that an increase in the charging current would create a corresponding increase in the amount of hydrogen entering the sample. The 12-h hold time at each current density value was determined to be sufficient to allow the hydrogen concentration to become equilibrated throughout the weld sample.[7] The testing parameters (Δi, i_{max}, solution) used for each sample varied due to time constraints and the fact that failure could not be induced. Testing was limited to surplus samples from the SSC study and could not be conducted on each weld condition. Table 4 presents the cathodic charging conditions that were used for the various weld conditions.

Two samples were originally tested in the NACE solution without the sodium arsenite addition. Sodium arsenite was added prior to impressing the large cathodic currents (up to 3 mA/cm^2) in an attempt to cause fracture. These currents were maintained for 24 h.

RESULTS

Hardness Mapping

Table 2 presents the HV and HRC hardness data produced from the hardness mapping investigation. There is a general reduction in peak sample hardness from Condition I through Condition III in both materials, indicating that the change in welding parameters had the desired effect. The hardness mapping results are discussed elsewhere.[7-8]

SSC

Results of the SSC testing were grouped as discussed based on three evaluation criteria as follows: double-ended fracture or samples that experienced complete separation, NACE criterion failure, and internal investigation. The results of the SSC evaluation are summarized and reported in the full SSC failure matrix in Table 5.

Double-Ended Fracture — All samples that fractured into two parts (double-ended fracture) exhibited the same general cracking morphology, which is shown in Figure 5. A surface-initiated thumbnail crack propagated by a brittle fracture mode (B) perpendicular to the applied stress until it reached a critical size. Ductile (D) rupture characterized by a ductile dimple fracture surface then occurred, usually at 45° to the tensile axis. This general fracture morphology was exhibited regardless of whether fracture initiated in the base metal (BM), fusion zone (FZ), or heat-affected zone (HAZ). In fractures that initiated in the FZ or a HAZ region, final ductile rupture always occurred in the FZ.

Post-fracture exposure of the fracture surface to the corrosive solution caused the formation of an iron sulfide corrosion product in most cases, making determination of fracture mode at times difficult or impossible in the SEM. Some detailed transgranular features were observed in samples that were removed shortly after failure. Intergranular cracking features were more easily discerned. The complete

TABLE 5

Results of SSC Test Matrix. Peak HV-10 kg Hardness is Given for Each Weld Condition.

X70 I High Hardness 310 HV		
	80% Yield	**100% Yield**
10% H_2S	FN-HAZ	DEF-HAZ
30% H_2S	FN-HAZ	FN-HAZ
100% H_2S	FN-HAZ	FI-HAZ

X80 I High Hardness 293 HV		
	80% Yield	**100% Yield**
10% H_2S	FI-BM	P
30% H_2S	DEF-BM	P
100% H_2S	FN-HAZ	DEF-HAZ

X70 II Medium Hardness 269 HV		
	80% Yield	**100% Yield**
10% H_2S	FI-BM	FI-BM
30% H_2S	P	P
100% H_2S	FI-FZ	DEF-FZ

X80 II Medium Hardness 286 HV		
	80% Yield	**100% Yield**
10% H_2S	P	FI-BM
30% H_2S	FI-BM	DEF-HAZ
100% H_2S	DEF-HAZ	DEF-HAZ

X70 III Low Hardness 236 HV		
	80% Yield	**100% Yield**
10% H_2S	P	FI-HAZ
30% H_2S	P	FI-HAZ
100% H_2S	P	FN-FZ

X80 III Low Hardness 247 HV		
	80% Yield	**100% Yield**
10% H_2S	P	DEF-HAZ
30% H_2S	FI-BM	DEF-HAZ
100% H_2S	P	DEF-HAZ

FN: failure by NACE criteria; HAZ: heat-affected zone; DEF: double-ended facture; FI: failure by internal investigation; BM: base metal; P: pass; FZ: fusion zone.

fractures are denoted in the full SSC failure matrix in Table 5.

There was one X80 base metal (BM) double-ended fracture (X80 I, 30% H_2S, 80% YS)—all other fractures occurred within the welds or HAZ. In the X70 I complete fracture, the initiation region corresponded to the location of maximum hardness determined from weld hardness mapping, which was the coarse grain heat-affected zone (CGHAZ).[7-8] The multi-pass welding used for the final welds created complex HAZ subregions that have been discussed in the literature.[12] A detailed description of the microstructures of the various zones in the welds used in this study is given elsewhere.[7-8] The X70 II sample exhibited the only FZ fracture initiation. Repeat tests were performed on each weld condition at 100% YS and 100% H_2S to determine the repeatability of NACE test method for welded samples. The results are discussed elsewhere.[7]

Metallographic cross-sectioning of each crack initiation region allowed for determination of the initiation microstructure and, when possible, the probable fracture mode (intergranular, transgranular, or ductile). The fractures were lapped down to the initiation point resulting in a small sampling of the total fracture surface. However, coupled with the SEM investigation, most fractures were well characterized.

Transgranular cracking was the predominant fracture initiation mode in the double-ended fractures. Intergranular fracture initiation was usually associated with the CGHAZ and was the sole fracture mode observed in the X70 Condition I weld, even when cracks propagated through the intercritically reheated coarse grain HAZ (IRCG). Propagating cracks often adopted mixed fracture modes; intergranular cracking was associated with the CGHAZ, while transgranular cracking occurred predominantly in the IRCG of the softer weld conditions. An example of documented intergranular cracking through the IRCG appears in Figure 6. This fracture mechanism may be attributed to the martensite austenite (MA) constituent lining the prior austenite grain boundaries in the IRCG. Transgranular cracking is evident

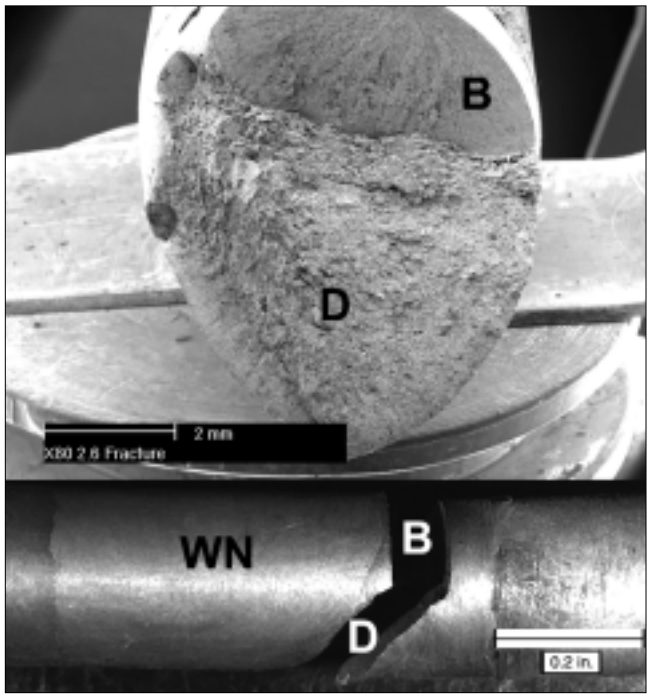

FIGURE 5. *Typical complete fracture morphology. B: brittle area; D: ductile rupture; WN: weld nugget.*

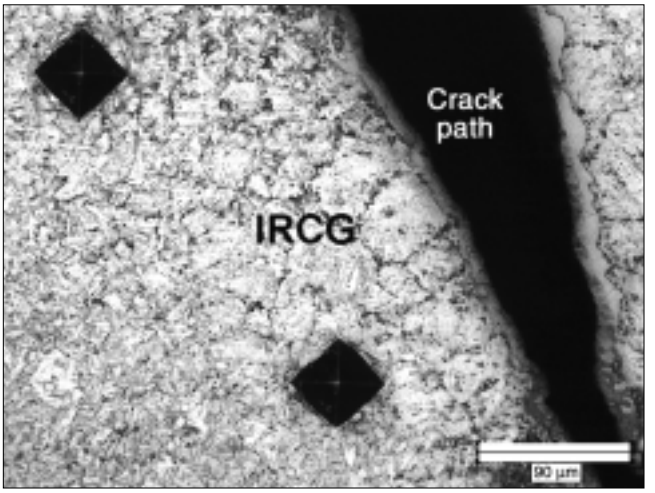

FIGURE 6. *Example of intergranular cracking in the intercritically reheated coarse grain heat-affected zone (IRCG). Note that the crack path is coated with a layer of electroless Ni for edge retention.*

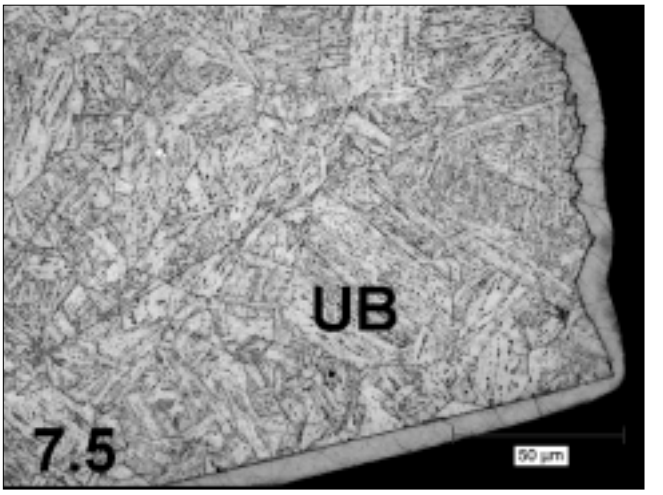

FIGURE 7. *Example of transgranular cracking through upper bainite (UB). The surface of the sample was coated with electroless Ni. The crack path is along the right side of the structure; the bottom was polished flat.*

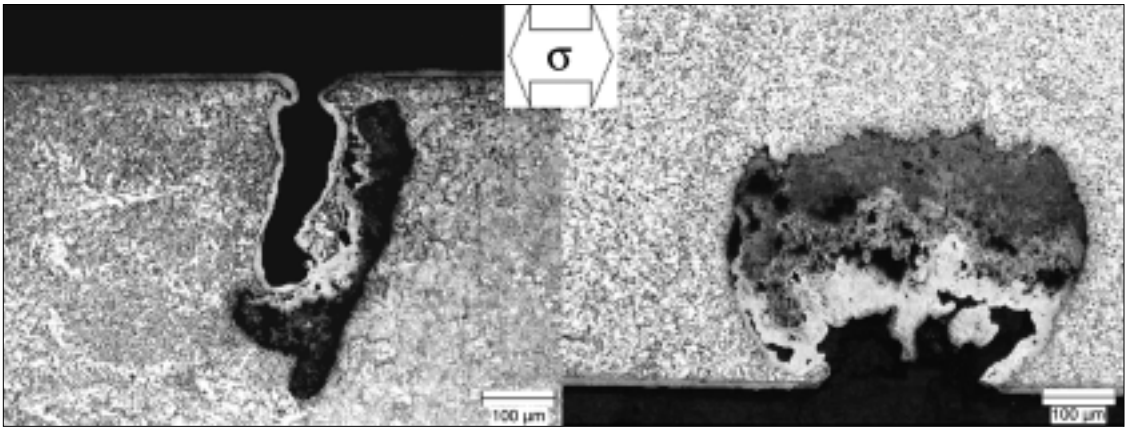

FIGURE 8. *Examples of pit-like attack revealed by metallographic sectioning.*

along the crack path through upper bainite (UB) shown in Figure 7. The most severe X70 II test condition (100% YS, 100% H_2S) produced crack initiation in the fusion zone (FZ) and propagation along the fusion boundary.

Crack initiation regions varied between the CGHAZ and IRCG in the X80 Condition I and II welds. Cracking initiated in the IRCG in all X80 III welds and propagation also occurred through this weld region. The most severe test (100% YS, 100% H_2S) conditions produced brittle crack propagation through the fusion zone in the X80 I and II welds. FZ crack propagation adopted an intergranular morphology in the FZ coarse grain HAZ (FZCG). Complete fracture in the weld was caused only by an applied stress equivalent to 100% of the specified parent material minimum yield strength for all weld conditions. The X80 welds were much more susceptible to complete failure, as they constituted a majority of the double-ended fractures.

NACE Criterion Failures — The complete separation fractures described above clearly failed according to the NACE TM0177 crack/no crack failure criterion. However, failure determination in the remaining samples proved more elusive using the NACE TM0177-A specification, which requires that any external cracking observed at 10X should be verified metallographically, with an SEM, or with mechanical testing. Difficulties arose with this failure determination due to the fact that severe "pitting" occurred in many of the samples. The extent of these "pits" was revealed upon metallographic sectioning. Most "pits" severely undermined the sample surface, and they appeared more crack-like on the outer surface. Figure 8 displays some general examples of the encountered "pit-like" damage. It should be noted

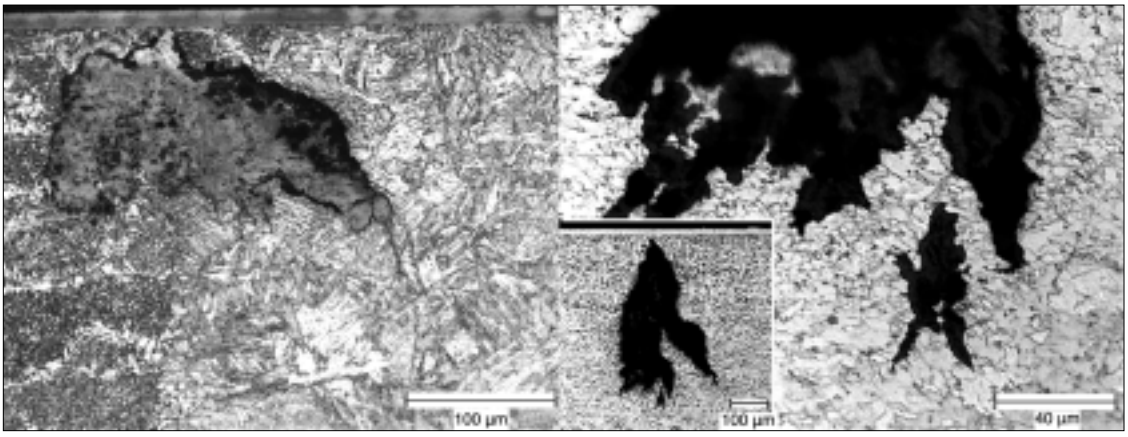

FIGURE 9. *Examples of pit-like attack with cracking features.*

that the standard usage of the term "pitting" refers to the localized breakdown of a thin protective passive film. Such films do not form on carbon steels at low potentials in acidic sour environments. The observed attack might be better described as localized general corrosion that occurs at a break in the somewhat protective iron sulfide film. Nonetheless, the term "pitting" was used.

Clearly, the examples in Figure 8 contain no evidence of SSC, which is required for a FAIL designation. The difficulty in failure determination arises, however, when these "pits" have crack-like features extending into the sample interior. This raises the question of whether existing terminal cracks created the pits, or if the pits created the cracks due to a stress riser effect. For this study, samples with pit-like attack containing terminal cracking features (like those in Figure 9) were designated as a FAIL. Pits with no indications of cracking were considered to be NO FAIL, passing the SSC test.

The X70 and X80 NACE TM0177 failure results that appear in Table 5 include the peak sample hardness values determined from hardness mapping studies performed on welded cross sections.[7-8] HV 10-kg testing adjacent to an internal crack in the X70 CGHAZ weld subregion indicated hardness of 310 HV, which is well above the HV 295 peak determined from weld hardness mapping prior to testing. Strain localization would not be expected to alter the post-fracture HV testing in this zone because the CGHAZ is typically the hardest, and therefore the most resistant to permanent deformation. The difference in the hardness measurements reflects the natural limitation of any hardness mapping technique to sample all areas of the weld, especially in the Condition I CGHAZ, where the hardness gradient is very steep.

The X70 failure results indicate that, while the high hardness weld condition (Condition I) failed under nearly all test conditions, the Condition II weld only failed under the most extreme testing conditions (100% YS, 100% H_2S). This was also true for the Condition III weld. The Condition II weld, with a peak hardness of ~270 Vickers, exceeded the 248 HV (HRC 22 equivalent) threshold.

Table 5 shows that the X80 Condition I weldment tolerated the 10% H_2S exposure. The failure in X80 Condition I (80% YS, 30% H_2S) might have been anomalous. This sample failed completely in the base metal, not in the weldment, and was the only sample to do so. It is surprising that more samples did not fail in the base metal, considering the relatively high applied stresses. X80 Condition II also exhibited some resistance at lower stresses and low H_2S concentrations. The X80 Condition III weld was not resistant at 100% YS in any test solution, possibly implicating the effect of plastic deformation, as the high heat input softened the HAZ to hardness levels significantly below that of the parent X80 material.[7-8]

Internal Investigation Failures — The internal investigation results are based on damage that was metallographically isolated using three search criteria. These include the following: cracking encountered during periodic metallographic sectioning when surface cracking at 10X was not observed, cracks encountered only during examination in the SEM, and internal damage encountered during the isolation of NACE cracks that was not directly associated with the optically visible surface cracking. This in-depth investigation revealed damage that would have gone unnoticed had only the NACE TM0177 failure criteria been implemented.

Not all cracking in the X70 welds indicated an SSC mechanism, as hydrogen-induced cracking (HIC) was encountered in the base metal CSR and the IRCG (Figure 10). Both their association with banded X70 parent microstructure and their parallel orientation relative to the applied stress characterized these cracks as HIC. SSC was also observed in the CSR

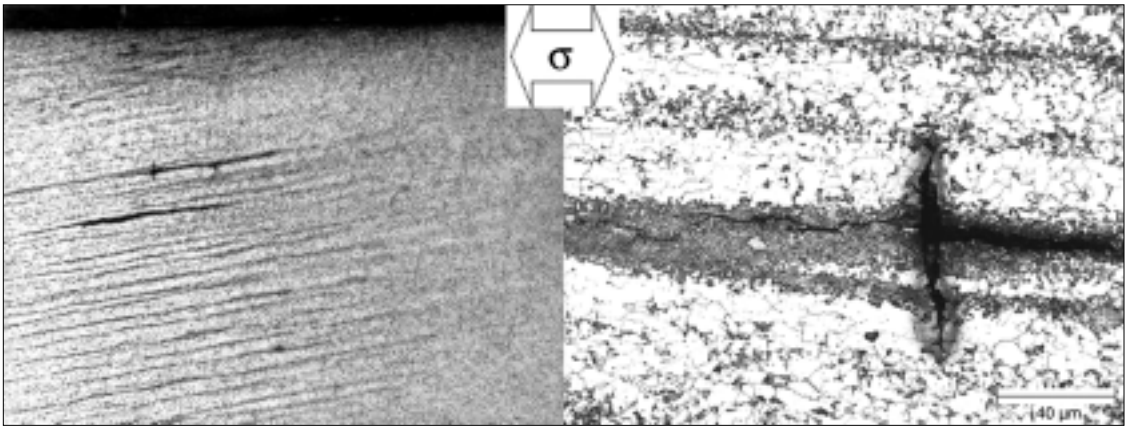

FIGURE 10. *Example of HIC cracks in X70 associated with the CSR. On the left, the cracks are seen to align with the bands in the microstructure. On the right, horizontal crack is aligned with bands and is parallel to stress direction. Vertical crack is SSC.*

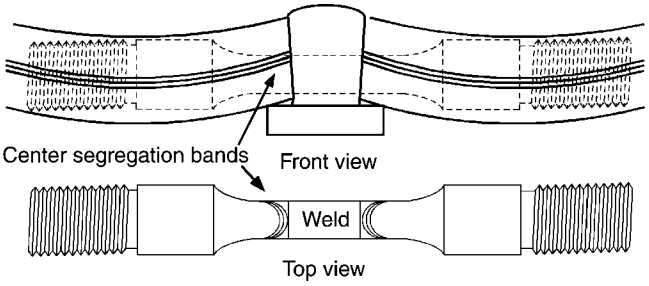

FIGURE 11. *Schematic representation of how center segregation bands are exposed at the gauge section surface during machining of tensile samples.*

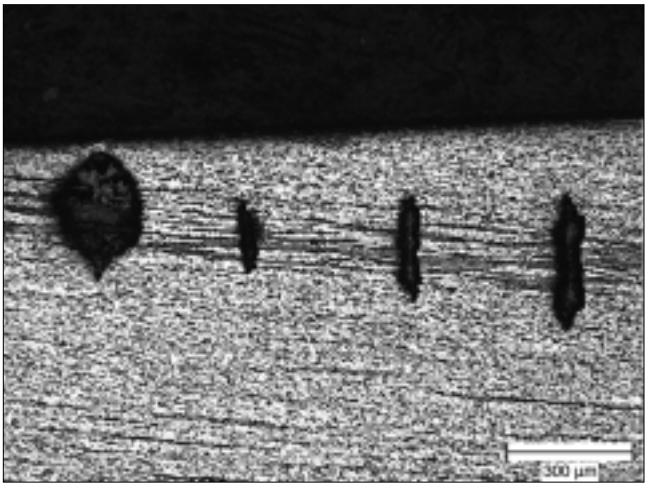

FIGURE 12. *Sulfide stress cracks associated with the CSR where it intersected the surface.*

region, sometimes in combination with HIC (Figure 10). The presence of the CSR in the X70 parent material influenced the forms of damage in X70 welded samples during the SSC testing. The localized attack was observed in samples where the CSR region intersected the sample surface and, therefore, was exposed to the H_2S-containing solution. Figure 11 shows how the weld orientation and machining produced samples with the CSR intersecting the exposure surface. Examples of the severe localized attack at the intersection of the CSR with the surface appear in Figure 12. Failures that occurred as a result of base metal cracking in Table 5 predominately account for the difference between the NACE failure determination and the internal investigation, especially in the X80 samples.

Internal cracks associated with the CSR were also found. These cracks were SSC in nature and were characterized by small cracks in the carbide and segregant-rich bands, oriented perpendicular to the applied stress direction (Figure 13). They occurred where (and if) the CSR intersected the intercritical HAZ (ICHAZ).

Corrosion Rate — The corrosion penetration rate in mils per year (mpy) was determined for each SSC sample using weight loss.[13] Crevice attack was noted on the tensile shanks of all exposed samples and occurred due to the crevice created by the exposure cell, which is the exact cell recommended by NACE TM0177-96.[5] The severity of crevice attack varied from sample to sample. Crevice attack not only altered the validity of the corrosion rate data, but also may have increased the cathodic current density on the gauge that was exposed to the bulk sour electrolyte.

DISCUSSION

NACE TM0177-A is geared toward the testing of homogenous samples and does not address specifically the testing of welded samples.[5] Therefore, the testing results must be viewed in the context of the

influences of welding, in particular the resulting local variations in microstructure and composition. Weld microstructure can change considerably over small length scales, especially in the HAZ. Because SSC cracking is usually associated with HAZ,[14] and these regions are very narrow in HSLA welds, HAZ cracking may be more difficult to detect than in a homogenous sample, where cracking is equally likely at any location in the gauge (since the microstructure is the same throughout) and more likely to grow to visible detection limits. The likelihood of crack termination is increased by the presence of a weld, because cracks can grow in an embrittled weld microstructure and then arrest in the base metal, or another less susceptible region. This may reduce the likelihood of complete, double-ended fractures, whose failure status is obviously very easy to determine when compared to terminal cracks. The problems detecting cracks in welds using the TM0177 failure criteria were addressed by the use of the more detailed internal investigation. The NACE criteria were actually less effective for locating cracks in the base metal than those associated with the weldments, as evidenced by the several base metal failures determined from the internal investigation alone (Table 5).

X70 — Internal investigation was necessary to determine four weldment failures and two base metal failures in X70. The base metal failures in the X70 samples were associated with the CSR, where it emerged on the sample surface. The internal SSC cracking at the CSR/ICHAZ intersection in the X70 welds was only detected using the in-depth internal investigation, not the NACE method. Therefore, several internal metallographic cross sections may be required to detect this form of SSC in carbon steel plate welds in which the base alloy contains a CSR.

In general, the X70 welds (excluding parent material failures) exhibited an increase in SSC susceptibility with increased weld peak hardness, as would be expected based on the long-standing correlation between hardness and SSC susceptibility.[4] The X70 Condition I weldments proved highly susceptible to SSC, more so than any other tested weld condition. This weld was made without preheat and generated the highest hardness measurement (310 HV). The high hardness CGHAZ was predominantly implicated in both complete fractures and terminal cracking. Generally, post-test hardness testing showed good agreement with the hardness mapping results, except for the X70 I welds as discussed above and the X80 III welds as discussed below. The X70 II welds (15.1 kJ/in., 250°F), which contained hard regions exceeding 248 HV (HRC 22), failed in the standard TM0177 tests (100% H_2S) at both applied stresses, yet exhibited resistance with lower H_2S concentrations (10, 30% H_2S). The failures that did occur in the X70 II welds were in the base metal and fusion zone. The X70 III (<248 HV) welds exhibited no susceptibility at the lower applied stress (80% YS), yet failed under the more aggressive testing conditions at the high applied stress (100% YS). The failures in the X70 III welds were due to either weld inclusions or SSC at the IRCG/CSR interface. The Condition II and III welds were, to some degree, resistant to SSC, whereas the X70 I weld (310 HV 10-kg) was determined not to be suitable for sour service.

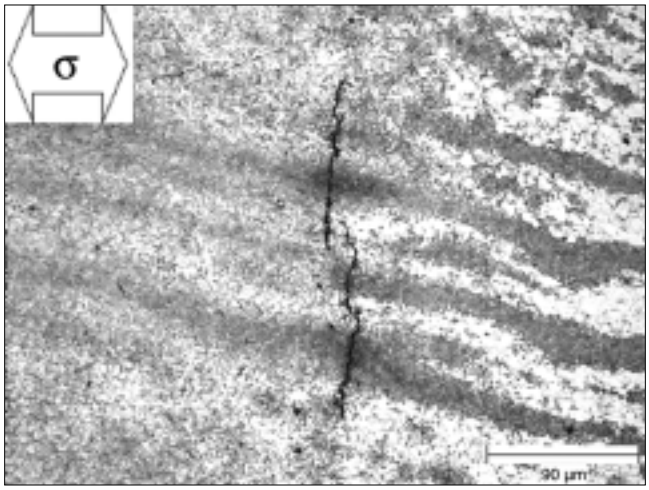

FIGURE 13. *Internal sulfide stress cracks at intersection of CSR and ICHAZ.*

X80 — Double-ended fractures accounted for a majority of the failures determined by the NACE criteria in the X80 welds. In fact, only one NACE failure was encountered that was not a double-ended fracture. The internal investigation, on the other hand, revealed X80 parent metal failures that were not detected using the NACE criteria. This was not expected because it was presumed that base metal cracking would be easily detected using the TM0177 criteria, especially since the standard is meant for testing homogenous samples. The base metal cracks that were not visible at 10X were usually discovered during the SEM examination of the sample surface.

The X80 welds exhibited very interesting trends when considering only those failures that occurred in welded regions (not base metal failures). Increasing hardness tended to increase resistance to SSC, especially at the applied stress equivalent to 100% of the specified minimum yield of the parent material (80 ksi). The Condition I weld exhibited good resistance to the modified NACE TM0177 testing conditions (10%, 30% H_2S). The Condition II weld was more susceptible under more severe testing conditions, and failed at 100% YS, 30% H_2S, where the Condition I weld did not. The X80 Condition III weld (peak hardness of 247 HV) exhibited poor performance at 100% YS. The applied stress level dominated the SSC susceptibility. The fact that susceptibility increased with lower hardness for the same applied stress and H_2S conditions suggests that SSC suscep-

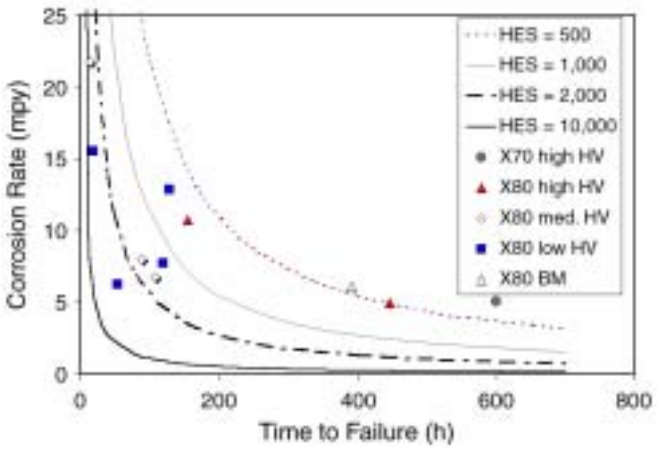

FIGURE 14. *HE susceptibility of fractured samples.*

tibility for the X80 welds might be controlled by localized ICHAZ and intercritically reheated (IRHAZ) softening, which was observed in the hardness mapping.[7-8]

Cracking Mechanism — Considering that the bulk of the literature maintains that SSC occurs by purely a HE mechanism, the time-to-failure (TTF) and cathodic charging results in this study raise some questions. The requirements for SSC based on the HE mechanism include a susceptible microstructure, a threshold level of hydrogen to induce cracking, and an applied or residual tensile stress.[15] It can be assumed that the cylindrical tensile bars used in the H_2S study exposed every weld microstructure directly to the test solution, so the most susceptible regions were exposed at the surface from the beginning of the test. Since the hydrogen enters the sample from the surface, the hydrogen concentration is highest at the surface as it diffuses inward. This is true even if the surface concentration decreases as the result of a decrease in the corrosion rate or change in the surface condition, such as the formation of an FeS film.[16] If every microstructure is indeed exposed at the cylindrical sample surface, including the most susceptible regions containing martensite-austenite constituent or centerline segregation, then these regions would be exposed to high hydrogen concentrations from the beginning of the exposure, and failure from HE should occur at short times. However, the values of TTF spanned a range from 12 h to 400 h (Figure 14). This is difficult to explain if only the HE mechanism were operating.

The long times to failure for the fractured samples may indicate that, in addition to the HE mechanism, there may be a strong anodic component in the failures observed in this study. Internal metallographic investigation exhibited extensive, pit-like attack in these samples. While these results suggest that dissolution played a role beyond providing electrons for the reduction of hydrogen, there is insufficient evidence to indicate that the mechanism involved anodic crack tip dissolution or stress corrosion cracking (SCC). It is possible that the pitting attack was of sufficient dimensions to create localized stress risers that initiated cracks and led to failure of the embrittled sample.

A dimensionless HE susceptibility parameter (HES) can help distinguish fractures that occur primarily due to HE from those that experience a mixed contribution from both anodic dissolution and HE. The dimensionless HES parameter incorporates the TTF and corrosion rate (CR):

$$HES = k\frac{r(in.)}{CR(mpy)\cdot TTF(h)} \quad (1)$$

where r, the gauge radius (0.25 in.), is a normalization value and k is a unit conversion constant ($k = 8.76 \times 10^6$ mpy-h/in.). A higher value of the HES parameter for a given fracture results from low corrosion rates and short failure times, and indicates a higher susceptibility to HE. The corrosion rate is directly proportional to the amount of hydrogen generated. Low values of HES, on the other hand, would be associated with longer failure times coupled with moderate corrosion rate, which implicates the role of dissolution.

Figure 14 displays the TTF vs CR data for all fractures. Iso-HES lines are plotted to compare the relative susceptibility of each fracture. The X80 II and X80 III welds are highly susceptible to HE, while the X70 welds (the two that failed) and the X80 I weld are more resistant. There was no apparent correlation between HES and either the % H_2S or the applied stress. This type of parameter may be useful for determining the susceptibility to HE under static loading conditions. However, the effect of crevice corrosion on both the measured CR (increased) and TTF (perhaps smaller owing to greater hydrogen evolution) must be considered. This approach ignores the different microstructures through which the cracks propagate, and this should not be disregarded. However, even the base metal failure took 392 h to fail. Nonetheless, the HES parameter presents a means for quantifying embrittlement susceptibility using a static test method. Currently, dynamic slow strain rate testing has been used to differentiate anodic stress corrosion cracking from HE.[17] The HES factor may be of utility in SSC studies or other HE investigations.

The results of the cathodic charging experiments also suggest that anodic dissolution plays a role in SSC. The applied galvanostatic step charging parameters described earlier were not sufficient to cause failure in samples that failed completely in testing involving H_2S. The identical solution (NACE solution + 2 mg/L $NaAsO_2$, no H_2S), in combination with an

impressed current of –140 μA/cm^2, created a steady-state hydrogen permeation flux equivalent to that produced at open circuit with the standard H_2S solution in a steel tested by Berkowitz and Heubaum.[1] All experimental cathodic currents eventually exceeded this current density, going to at least –625 μA/cm^2.

The hold time was even extended to 24 h for the highest applied currents. However, the cathodically charged samples did not fail. If the SSC mechanism relied solely on the concentration of absorbed hydrogen in the double-ended fractures, then the severe hydrogen charging conditions should have been sufficient to reproduce these failures. The impressed cathodic currents effectively eliminated anodic dissolution (especially at higher applied currents) and any possible anodic contribution to the cracking mechanism. Apparently, dynamic straining is required to embrittle cathodically charged samples, but static stress is sufficient in sour environments.

Extrapolation to Service — Due to the physical constraints that prevented the actual untempered cap passes from being isolated in the gauge sections of the tested tensile samples, it may not be prudent to extrapolate data from this study to in-service weld cap regions. This is particularly true for the X70 Condition I welds, which exhibited significant tempering responses as evidenced by the considerably lower peak sample hardness (310 HV) relative to the peak weld hardness (336 HV). Regardless, the X70 Condition I welds did not pass any SSC test, when considering both failure criteria. The use of the low heat input (15.1 kJ/in.) without preheat is not suggested for the X70 material in sour service. The X80 Condition I weld exhibited considerably lower tempering responses, such that the machined sample contained hardness similar to the hardest weld cap regions (only 2 HV difference). This weld condition exhibited base metal anomalous failures at 80% YS, but not at 100% YS (Table 5). The reason this occurred is unclear, because samples that failed at 80% YS would be expected to fail at even higher applied stresses.

Heeding the failures determined according to the NACE criteria and internal investigation, yet ignoring the base metal failures, both the X80 Condition I and X70 Condition II welds were resistant to SSC in the 10% and 30% H_2S solutions. Additionally, the X80 Condition II weld was resistant in only the 10% H_2S solution. The base metal failures in the X70 I and II welds were attributed to surface emergence of the CSR. This region would not be directly exposed to the service environment in a welded service pipe.

Assuming that the reduction in the dissolved H_2S in the NACE solution produces a corresponding reduction in the absorbed hydrogen content in the SSC test samples, it may be possible to predict the locations in an in-service pipe wall where elevated hardness (>HV 248) can be tolerated. Asahi, et al.,

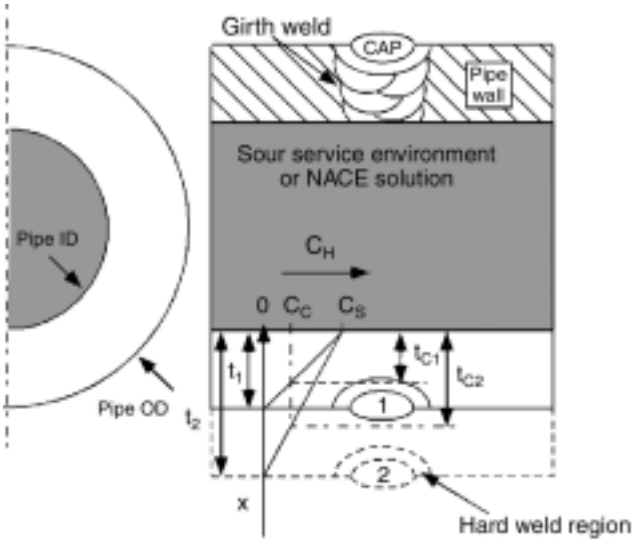

FIGURE 15. *Schematic representation of how the results can be extrapolated to sour service.*

determined a correlation between the absorbed concentration of hydrogen, C_H, solution pH, and the concentration of H_2S in solution to quantify the severity of a particular sour environment:[18]

$$C_H = K(H^+ \cdot H_2S)^{0.26} \quad (2)$$

where C_H is the H content of the steel (ppm), K is a constant that relates to the trapping density in the steel, H^+ is the H ion concentration of the solution ($\approx 10^{-pH}$), and H_2S is the concentration of H_2S in solution (ppm). Assuming that the steady-state concentration gradient across a pipe wall is linear, going to zero on the outer pipe surface, the concentration of hydrogen $C_H(x)$ at any distance x from the outer diameter (OD) pipe surface can be determined:

$$C_H(x) = \left(\frac{C_{H,s}}{t}\right) \cdot x \quad (3)$$

where $C_{H,s}$ is the concentration of hydrogen (ppm) at the inner surface exposed to the sour service environment and t is the wall thickness. Figure 15 schematically represents the situation. This approach neglects the effects of hydrogen trapping on the concentration profile, ignores any rate limiting step created by the desorption of hydrogen from the outer pipe wall, and assumes that diffusivity is independent of concentration. For a pipe containing NACE solution saturated with H_2S, the concentration of H_2S in solution or the H_2S parameter in Equation (2) is 3,300 ppm.[6] If the concentration of hydrogen (C_H) increases linearly with distance from the OD surface, the diluted H_2S concentrations (10% and 30% H_2S) used in this investigation created experimental ana-

logs to two different *x* positions within the pipe wall. To determine the value of *x* at which the SSC-resistant welds would be tolerated in terms of the pipe wall thickness, t, Equation (2) is substituted for both $C_H(x)$ and $C_{H,s}$ in Equation (3), which is then rearranged to solve for *x*:

$$x = \left(\frac{(H_2S)_x}{(H_2S)_s}\right)^{0.26} \cdot t = \left(\frac{(H_2S)_x}{3{,}300\ ppm}\right)^{0.26} \cdot t \qquad (4)$$

The term $(H_2S)_x$ in the numerator is a variable that relates to the absorbed hydrogen concentration created by either of the diluted test solutions and corresponds to the concentration at a specific location in the full-scale pipe wall. The term in the denominator, $(H_2S)_s$ = 3,300 ppm, is the absorbed hydrogen concentration created at the inner pipe surface in contact with the process stream containing saturated H_2S. The H^+ factor drops out because the pH is identical in both the NACE solution and the hypothetical process stream.

If the concentration of H_2S (ppm) in one of the tests in this study for which a sample received a passing indication is inputted for the $(H_2S)_x$ value in Equation (4), then the resulting value of *x* can be used to determine the depth from the OD that the given microstructure with a given hardness could be expected to survive if the inside of the pipe were exposed to a 100% H_2S environment. For example, the 269 HV peak hardness in the X70 II samples that passed the 10% H_2S exposure (H_2S = 330 ppm) could be tolerated up to 0.55t in from the OD. Samples passing the 30% H_2S exposure (H_2S = 990 ppm) indicate that the peak weld hardness could be tolerated up to 0.73t in from the OD. Samples that passed the NACE TM0177 standard exposure (100% H_2S = 3,300 ppm), like the X70 and X80 Condition III welds at 80% YS, could tolerate direct contact with the solution in a full-scale test, if the residual stresses are not excessive.

The complex interactions among microstructure, corrosion, HE, and mechanical stress states make almost any experimental investigation of SSC in weldments very complicated. The simplified approach adopted by this investigation has several possible sources of inherent weakness. Of these, the most important limitations were on the inability of the dogbone tensile samples to isolate actual cap weld regions, the uncharacterized relationship between H_2S concentration and absorbed hydrogen content, and the duplication of residual weld stresses. In light of these limitations, and those present in other SSC studies, care should and must be taken when extrapolating laboratory testing results to anticipated service performance. The environmental, safety, and monetary implications of SSC service failures can be, to say the least, enormous.

CONCLUSIONS

❖ The susceptibility to SSC of welded X70 and X80 line pipe steel was studied under conditions of varying applied stress, H_2S concentration, and peak weld hardness. Several important observations were made in this work.
❖ Except for the internal SSC cracks associated with the CSR/weld intersection, the NACE TM0177 failure criteria were found to be adequate for detecting weldment cracks in narrow HAZ.
❖ A maximum hardness of 248 HV should be maintained for carbon steel parent materials and regions of carbon steel weldments that are in direct contact with sour service environments.
❖ A relaxation in the allowable hardness of outer cap regions in sour service girth welds is reasonable, as originally recommended by TWI, as long as the wall thickness is sufficient and the performance of the as-welded material is characterized with laboratory screening.
❖ The low-carbon (~0.03 wt% C) X80 steel was subject to HAZ softening relative to the base metal, which increased SSC susceptibility due to strain localization. A minimum HAZ hardness may be justified for these types of steels.
❖ The low-carbon (~0.03 wt% C) X80 steel was more resistant to SSC in the as-welded condition and tolerated much higher absolute tensile stresses than the as-welded X70 steel.
❖ SSC experiments showed that the CSR in controlrolled steels is susceptible to SSC, and may dictate both alloy and weld susceptibility. Cracking in the CSR went unnoticed when applying only the NACE failure criteria.
❖ Cathodic charging results, TTF observations, and an observed localized breakdown in the somewhat protective iron sulfide film suggest that there is an anodic component to SSC.
❖ Laboratory screening may permit the use of steel welds with regions exceeding 248 HV in sour service environments, provided these high hardness regions are not in contact with the sour environment and the local residual stresses are well characterized.

ACKNOWLEDGMENTS

This project was funded by an Edison Welding Institute Cooperative Research Program, 43564-IRP. The authors acknowledge personal contributions from C. Ribardo (formerly at EWI) and G. Todd (CC Technologies). CC Technologies donated the use of their laboratory facility for H_2S testing performed in this study. The welds were made by Edison Welding Institute.

REFERENCES

1. B.J. Berkowitz, F.H. Heubaum, Corrosion 40, 5 (1984): p. 240.

2. R.D. Kane, Int. Met. Rev. 30, 6 (1985): p. 291.
3. J.C. Turn, B.E. Wilde, C.A. Troianos, Corrosion 39, 9 (1983): p. 364.
4. NACE Standard Materials Requirements, "Sulfide Stress Cracking Resistant Metallic Materials for Oilfield Equipment" (Houston, TX: NACE International, 1994), p. 1.
5. NACE Standard Test Method, "Laboratory Testing of Metals for Resistance to Specific Forms of Environmental Cracking in H_2S Environments" (Houston, TX: NACE International, 1996).
6. R.A. Walker, The Significance of Local Hard Zones on the Outside of Pipeline Girth Welds (Cambridge, U.K.: The Welding Institute, 1989), p. 1.
7. G. Omweg, "Sulfide Stress Cracking Resistance of Welded High-Strength Low-Alloy Steels" (MS thesis, Materials Science and Engineering Department, The Ohio State University, 2001).
8. G.M. Omweg, G.S. Frankel, W.A. Bruce, G. Koch, Weld J. 82 (2003): p. 136-144S.
9. M.S. Cayard, R.D. Kane, Corrosion 53, 3 (1997): p. 227.
10. W.B. Morrison, "Status of Microalloyed (HSLA) Steel Development," eds. J.T. Hickey, D.G. Howden, M.D. Randall, Proc. Int. Conf. Metall., Weld., Qualif. Microalloyed (HSLA) Steel Weldments (Miami, FL: American Welding Society, 1990).
11. "Sulfide Stress Cracking Resistance of Pipeline Welds," Mater. Perform. 32, 1 (1993): p. 58-64.
12. D.P. Fairchild, N.V. Bangaru, J.Y. Koo, P.L. Harrison, A. Ozekcin, Weld. Res. 70 (1991): p. 321s.
13. D.A. Jones, Principles and Prevention of Corrosion, 2nd ed. (Upper Saddle River, NJ: Prentice-Hall, 1996), p. 572.
14. R.D. Kane, J.P. Ribble, M.J. Schofield, Weld. J. 70 (1991): p. 56.
15. H.H. Tang, M.S. Cayard, "Test Methods for the Evaluation of Materials for Wet H_2S Service," CORROSION/99, paper no. 421 (Houston, TX: NACE, 1999).
16. S.Y. Tsai, H.C. Shih, Corros. Sci. 38, 5 (1996): p. 705.
17. C.D. Kim, B.E. Wilde, "A Review of the Strain-Rate Stress Corrosion Cracking Test," Stress Corrosion Cracking—The Slow Strain-Rate Technique, in ASTM STP 665, eds. G.M. Ugiansky, J.H. Payer (West Conshohocken, PA: ASTM International, 1979), p. 97.
18. H. Asahi, M. Ueno, T. Yonezawa, Corrosion 50, 7 (1994): p. 537.

CORROSION RESEARCH CALENDAR

CORROSION is a technical research journal devoted to furthering the knowledge of corrosion science and engineering. Within that context, *CORROSION* accepts notices of calls for papers and upcoming research grants, meetings, symposia, and conferences. All pertinent information, including the date, time, location, and sponsor of an event should be sent as far in advance as possible to: Angela Jarrell, Managing Editor, *CORROSION*, 1440 South Creek Drive, Houston, TX 77084-4906. Notices that are not accompanied by the contributor's name, daytime telephone number, and complete address will not be considered for publication.

2003

July 14-17—RUST 2003, 13th U.S. Navy and Industry Corrosion Technology—Louisville, NY; Contact Don Hileman, E-mail: hilemande@nswcl.navy.mil; Web site: http://cte-online.org.

July 15-17—1st International Conference on Concrete Repair—St. Malo, Brittany; Contact Conference Secretariat, Phone: +44 (0) 208381 1429; E-mail: conference@concrete-testing.com.

August 10-14—SeaHorse 2003, The Marine Corrosion Conference—Wrightsville Beach, NC; Contact Lisa Weiss, Phone: 910/256-2271, ext. 300; E-mail: seahorse@laques.com; Web site: www.marine-corrosion.com.

August 18-20—2003 International Maintenance Conference—Chicago, IL; Contact Brent Lancaster, Phone: 704/547-6017; E-mail: blancast@epri.com; Web site: www.epri.com.

August 19-22—7th Corrosion and Protection Congress and 2nd International Materials Congress—Bucaramanga, Colombia; Contact Daria Pena, Phone: +57 7 6320471; E-mail: dypena@uis.edu.co.

August 21-22—Maritime Environmental Engineering Technical Symposium 2003—Arlington, VA; Contact Henry Wilson, 410/764-6065.

August 28-29—28th Conference on Our World in Concrete and Structures—Singapore; Contact Conference Secretariat, Phone: +(065) 67332922; E-mail: cipremie@singnet.com.sg; Web site: www.cipremier.com.

* **September 7-11—NACE Corrosion Technology Week—Pittsburgh, PA;** Contact NACE, 281/228-6200.

* **September 14-17—NACE Northern Area Eastern Conference—Ottawa, ON, Canada;** Contact Bruce Baldock, Phone: 613/998-4396; E-mail: bruce.baldock@nrc.ca.

September 15-18—The 2nd ASM International Surface Engineering Congress and Exposition—Indianapolis, IN; Contact ASM Customer Service, Phone: 440/338-5151, dial 6; E-mail: cust-srv@asminternational.org.

* **September 21-24—NACE Eastern Area Conference—Columbus, OH;** Contact Jeff Didas, Phone: 804/672-2718; E-mail: JDidas@colpipe.com.

September 28-October 2—Eurocorr 2003—Budapest, Hungary; Contact Erika Kalman, Phone: +36 1 3257548; E-mail: eurocorr@chemres.hu; Web site: www.chemres.hu/eurocorr.

* **October 5-9—NACE Central Area Conference—Houston, TX;** Contact Jane Brown, 713/468-4765.

October 6-8—Water Middle East 2003—Manama, Bahrain; Contact Amy Schur, Phone: 613/549-0404; E-mail: ah@unilinkfairs.com.

October 13-16—ASM International's Materials Solutions Conference and Exposition—Pittsburgh, PA; Contact ASM Customer Service, Phone: 440/338-5151, dial 6; E-mail: cust-srv@asminternational.org.

* **October 20-24—LATINCORR-2003, 5th NACE Latin American Region Corrosion Congress, 8th Ibero American Congress of Corrosion and Protection—Santiago, Chile;** Contact Laura Lillo, E-mail: lalillo@lauca.usach.cl; Web site: www.latincorr.cl.

October 26-30—SSPC Annual Conference—New Orleans, LA; Contact Rose Mary Surgent, Phone: 412/281-2331; Fax: 412/281-9993; E-mail: surgent@sspc.org.

November 11-13—3rd Stainless Steel World Conference and Expo, Maastricht, The Netherlands; Contact Sjef Roymans, Phone: +31 575 585286; E-mail: s.roymans@kci-world.com.

November 12-14—ICE 2003–FSCT 81st Annual Meeting and International Coatings Expo—Blue Bell, PA; Contact Mark Moon, Phone: 610/940-0777; E-mail: fsct@coatingstech.org.

* Sponsored or cosponsored by NACE International.